Experiments on the longitudinal ion momentum balance in a magnetized plasma

Experiments on the longitudinal ion momentum balance in a magnetized plasma

J. M. M. J. Vogels, J. C. M. de Haas, D. C. Schram, and A. Lunk[a)]
Eindhoven University of Technology, Physics Department, P. O. Box 513, 5600 MB Eindhoven, The Netherlands

(Received 4 June 1985; accepted for publication 7 August 1985)

In the magnetized plasma of a hollow cathode arc the longitudinal and rotational drift velocities of ions have been measured, together with the electron and neutral densities and the temperatures of ions, electrons, and neutrals. The radial and longitudinal gradients of these quantities have been established. The ions drift against the electric field towards the anode with velocities between about 500 and 2500 m/s, driven by the plasma pressure gradient which is balanced by viscous deceleration and by friction against the surrounding neutral gas. The classical theory of the momentum balance with a turbulent contribution to the viscosity provides a good description of the longitudinal ion transport and explains direction and magnitude of the occurring drift velocity.

I. INTRODUCTION

In a magnetized plasma column the ion drift velocity is an important quantity. Plasma rotation has been studied by several authors.[1–4] One of the motivations is the possible use of a plasma centrifuge for element or isotope separation.[5–11] Also, in several laser plasmas particle transport processes are dominant.[12] Recently several schemes have been investigated for the use of plasmas in particle sources. Both beam sampling techniques[13–15] and high-energy beam production for neutral injection in thermonuclear plasmas,[16–19] are drawing attention.

In thermonuclear plasma physics the radial confinement time plays a decisive role in the energy efficiency of fusion reactions (Lawson criterion). It has been argued that both turbulent diffusion[20] and the drift as a consequence of neutral particle friction in the presence of a magnetic field,[21] depend on ion drift velocities. The toroidal and the poloidal ion drift velocity in a tokamak have been measured.[22,23] The diamagnetic drift dominates the poloidal rotation.

We are interested in the ion drifts in a hollow cathode arc (HCA),[24,25] especially the longitudinal drift. Measurements by several authors[26–29] indicate the dominance of the E/B drift, with an inwardly directed E field, over the diamagnetic drift. In the HCA the ion rotation velocity is about 30% to 50% of the ion thermal speed v_{ti}.

The HCA is an excellent plasma for the study of the longitudinal drift velocity and momentum balance of the ions, especially because axial gradients are involved. We describe our study of the axial ion momentum balance in an argon arc. The momentum balance is analyzed experimentally in combination with the theoretical approach by Braginskii.[30] We measure not only longitudinal ion flow but also rotation, particle densities and temperatures. We scan both over longitudinal and lateral positions. The different terms in the momentum balance are calculated on the basis of our experiments. Plasma pressure, plasma velocity, inertia, and neutral friction, including charge exchange and ionization, are the terms of interest.

a) Permanent address: Ernst-Moritz-Arndt Universität, Greifswald (GDR).

II. THEORY OF THE AXIAL MOMENTUM BALANCE

For the description of the axial momentum balance we use Braginskii's model.[30] We assume rotational symmetry and stationary conditions. We add to it a frictional term for ionizing and elastic collisions with neutrals. The addition is allowed because these collisions are much less frequent than collisions among ions or electrons and do not effect appreciably the electron or ion velocity distribution.[29] The continuity equations read

$$\nabla \cdot (n\mathbf{w})_{e,i} = S = n_a n_e \langle \sigma_{\text{ion}} v_e \rangle. \tag{1}$$

Here n denotes the particle density, $\mathbf{w}$ the drift velocity, σ_{ion} the ionization cross section, v the particle random velocity, and S the source term. We use the subscript e for electrons, i for ions, and a for neutrals. In S both direct and stepwise ionization is comprised, but recombination may be neglected.[31]

Now we may derive a longitudinal momentum balance equation for the electron-ion mixture. It may be expected that the mutual momentum interactions between ions and electrons will cancel. As we will see also the electric field will disappear out of the momentum balance of the mixture because of its electrical neutrality. Therefore the ions may drift towards the anode. First we write the momentum balances of the charged particle species:

$$[\nabla \cdot (nm\mathbf{ww})]_z = nq(E_z + w_r B_\theta) - (\partial/\partial z) n k_B T - (\nabla \cdot \Pi)_z + F_z - M_z'^a + m w_{za} S. \tag{2}$$

Here Π is the viscosity tensor and $M_z'^a$ is the neutral friction by ion-neutral collisions only. The particle mass is m, q is the charge, E the electric field, B the magnetic field, k_B the Boltzmann constant, T the temperature. The radial, angular and longitudinal coordinates are r, θ, and z, respectively. The latter is 0 at the cathode and increases towards the anode.

The F_z denotes the interactions between the electrons and the ions. It consists of the friction by electrical resistivity and of two temperature gradient (Nernst) terms:

 0021-8979/86/010071-09$02.40

$$F_z = -\frac{qnJ_z}{\sigma_\parallel} + 0.71\frac{q}{|q|}n\frac{\partial}{\partial z}k_B T_e$$
$$-\frac{3}{2}\frac{q}{|q|}\frac{n}{\Omega_e\tau_e}\frac{B_\theta}{B_z}\frac{\partial}{\partial r}k_B T_e\ . \tag{3}$$

The $\sigma_\parallel$ is the electric conductivity parallel to B, Ω is the cyclotron angular frequency and τ is the momentum collision time; J is the current density.

We simplify Eq. (2) by combining it with Eq. (1):

$$nm\left(w_r\frac{\partial}{\partial r}+w_z\frac{\partial}{\partial z}\right)w_z = nq(E_z + w_r B_\theta) - \frac{\partial}{\partial z}nk_B T$$
$$-(\nabla\cdot\Pi)_z + F_z - M_z^a, \tag{4}$$

with for the ions

$$M_{zi}^a = M_z'^a + m_i(w_{zi} - w_{za})S$$
$$= m_i(w_{zi} - w_{za})n_a(n_i\langle\sigma v\rangle_{ia} + n_e\langle\sigma_{\rm ion}v_e\rangle). \tag{5}$$

The σ (without subscript) is the cross section for charge exchange and elastic collisions.

The ion frictional term M_{zi}^a now contains contributions of ionization, charge exchange, and elastic collisions. We suppose the ions to be singly charged ($q_i = e$) and since the plasma is quasineutral it follows that $n_e = n_i$. Because $\Omega_e\tau_e \gg 1$ and $|w_e| \ll v_{te}$, with $v_t = (2k_B T/m)^{1/2}$, the electron viscosity is negligible[30] as is also M_{ze}^a.

The momentum balance of the electron-ion mixture is obtained by the elimination of the mutual interactions in F_z [Eq. (3)]. We neglect the electron inertia with respect to their pressure gradient, which is justified because $(w_{ze}/v_{te})^2 \ll 1$, and a summation of the two equations in Eq. (4) yields

$$nm_i\left(w_{ri}\frac{\partial}{\partial r}+w_{zi}\frac{\partial}{\partial z}\right)w_{zi} = J_r B_\theta - \frac{\partial}{\partial z}nk_B(T_e + T_i)$$
$$-(\nabla\cdot\Pi)_{zi} - M_{zi}^a. \tag{6}$$

We note that the E_z field has disappeared; it only affects the mutual interactions (F_z) but not the longitudinal momentum of the quasineutral mixture.

The ion drift velocity w_{zi} is in an excellent approximation to the longitudinal center of mass velocity of the plasma: $w_{zp} = (m_i w_{zi} + m_e w_{ze})/(m_i + m_e)$. As we will see $w_{zi} \simeq 10^3$ m/s and $w_{ze} \simeq 10^4$ m/s; because further $m_i/m_e = 7\times 10^4$ the relative deviation $(w_{zp}/w_{zi} - 1) \simeq 10^{-4}$.

The radial ion flux follows from Eq. (1):

$$nw_{ri} = \frac{1}{r}\int_0^r r'\left(S - \frac{\partial}{\partial z}nw_{zi}\right)dr'. \tag{7}$$

The validity of our considerations is confined to plasmas with a radius larger than the smaller of the ion mean free path and the ion cyclotron radius.[29,30] As stated before also the collision times between the charged particles should be much shorter than those of elastic and charge exchanging collisions or ionizations.

We discuss now the different momentum contributions. The magnitude of each term of Eq. (6) will be compared with the plasma pressure gradient $\partial p/\partial z$ with $p = nk_B(T_e + T_i)$. The characteristic lengths will be denoted Z and R: $\partial/\partial z \sim 1/Z$ and $\partial/\partial r \sim 1/R$ with $10^{-2} < R/Z < 10^{-1}$. The temperatures T_i and T_e are of the same order of magnitude.

A. Inertia

For the relative momentum contribution containing w_{ri} we may write

$$\frac{nm_i w_{ri}(\partial/\partial r)w_{zi}}{(\partial/\partial z)nk_B(T_e + T_i)} \sim \frac{w_{ri}w_{zi}Z}{v_{ti}^2 R} \tag{8a}$$

and for the other term

$$\frac{nm_i w_{zi}(\partial/\partial z)w_{zi}}{(\partial/\partial z)nk_B(T_e + T_i)} \sim \frac{w_{zi}^2}{v_{ti}^2}. \tag{8b}$$

As we will see both contributions may only be significant near the cathode.

B. Poloidal B field

The $J_r B_\theta$ is zero on the axis and far from the axis it is negligible:

$$\frac{J_r B_\theta}{(\partial/\partial z)nk_B(T_e + T_i)} \sim \frac{ew_{ri}\mu_0 I_a Z}{2\pi R m_i v_{ti}^2} \sim 10^{-2}. \tag{9}$$

Here μ_0 is the magnetic permeability and I_a the arc current.

C. Viscosity

The axial component of the ion viscosity can be written as[30]

$$(\nabla\cdot\Pi)_{zi} = \frac{2}{3}\frac{\partial}{\partial z}\left(\eta_0\frac{\partial}{\partial r}w_{ri} + \eta_0\frac{w_{ri}}{r} - 2\eta_0\frac{\partial}{\partial z}w_{zi}\right)$$
$$-\frac{1}{r}\frac{\partial}{\partial r}r\eta_2\left(\frac{\partial}{\partial r}w_{zi} + \frac{\partial}{\partial z}w_{ri}\right) \tag{10}$$
$$-\frac{1}{r}\frac{\partial}{\partial r}r\eta_4\frac{\partial}{\partial z}w_{\theta i}.$$

Here the viscosity coefficients η_k are $\eta_k = n_i k_B T_i \tau_{ii} \times f_k(\Omega_i\tau_{ii})$ with $f_k \lesssim 1$ for all k and τ_{ii} according to

$$\tau_{ii} = \frac{(\hat{T}_i/1V)^{3/2}}{7.59\times 10^6 \hat{n}_i(\ln\Lambda_c/10)}. \tag{11}$$

Here $\hat{T}_i = k_B T_i/e$ and $\hat{n}_i = n_i/(10^{20}\ {\rm m}^{-3})$; $\ln\Lambda_c$ is the Coulomb logarithm[32] ($\ln\Lambda_c \simeq 10$); $\hat{\tau}_{ii} = \tau_{ii}/(1\ {\rm s})$. We will estimate the magnitudes of the terms in Eq. (10) with respect to the $(1/r)(\partial/\partial r)r\eta_2(\partial/\partial r)w_{zi}$ term. In the same sequence of the terms

$$\frac{(\nabla\cdot\Pi)_{zi}}{\frac{1}{r}\frac{\partial}{\partial r}r\eta_2\frac{\partial}{\partial r}w_{zi}} \sim \frac{[(w_{ri}R/w_{zi}Z) + (w_{ri}R/w_{zi}Z) - (R^2/Z^2)]}{\ll 1}$$
$$-\frac{[1 + (w_{ri}R/w_{zi}Z)]}{\ll 1} - \frac{-(w_{\theta i}R/w_{zi}Z)}{<1} \tag{12}$$

These estimates are valid unless $f_2 \ll 1$, so if $\Omega_i\tau_{ii} < 10$ [see Eq. (14a)]. For higher values of $\Omega_i\tau_{ii}$ however classical viscosity can play no role at all in the axial momentum balance of the HCA. From Eq. (12) we conclude that

$$(\nabla\cdot\Pi)_{zi} \simeq -\frac{1}{r}\frac{\partial}{\partial r}r\left(\eta_2\frac{\partial}{\partial r}w_{zi} + \eta_4\frac{\partial}{\partial z}w_{\theta i}\right) \tag{13}$$

with[29]

$$f_2 = \frac{1.2(\Omega_i \tau_{ii})^2 + 2.23}{(\Omega_i \tau_{ii})^4 + 4.03(\Omega_i \tau_{ii})^2 + 2.33} \tag{14a}$$

and

$$f_4 = \frac{(\Omega_i \tau_{ii})^3 + 2.38(\Omega_i \tau_{ii})}{(\Omega_i \tau_{ii})^4 + 4.03(\Omega_i \tau_{ii})^2 + 2.33}. \tag{14b}$$

The relative magnitude of the viscosity in Eq. (6) in the case when $\Omega_i \tau_{ii} < 10$ is

$$\frac{(\nabla \cdot \Pi)_{zi}}{(\partial / \partial z)p} \sim \frac{w_{zi} l_{ii} Z}{v_{ti} R^2} \sim 1, \tag{15}$$

with $l_{ii} = v_{ti} \tau_{ii}$. We conclude that the kinetic viscosity plays a role comparable with the pressure gradient.

D. Ionization and neutral friction

We discuss the reaction rates $\langle \sigma v \rangle_{ia}$ and $\langle \sigma_{\text{ion}} v_e \rangle$ in Eq. (5). For the direct ionization from the neutral ground level we use the formula for $\sigma(v_e)$ by Drawin[33] which is integrated numerically to give the rate coefficient $\langle \sigma_{\text{ion}} v_e \rangle_{\text{dir}}$ (Fig. 1). For further calculations we fit an analytic expression to the obtained rate coefficient, which is multiplied by a factor 1.74 to account for stepwise ionization. The value of 1.74 serves as an approximation except at $\hat{T}_e = 4$ V and $\hat{n}_e = 0.8$ for which it has been calculated.[34,35]

The frictional term $\langle \sigma v \rangle_{ia}$ is made up of charge exchange and elastic collisions. Under most of our conditions $v_{ti} \gg v_{ta}$ so we put $v = v_i$. According to Kobayashi[36] in the ion energy range between 0.2 and 5 eV a constant charge exchange cross section of 5.10×10^{-19} m^2 can be used. The elastic cross section is smaller[37] and has a value of 1.7×10^{-19} m^2. The result is

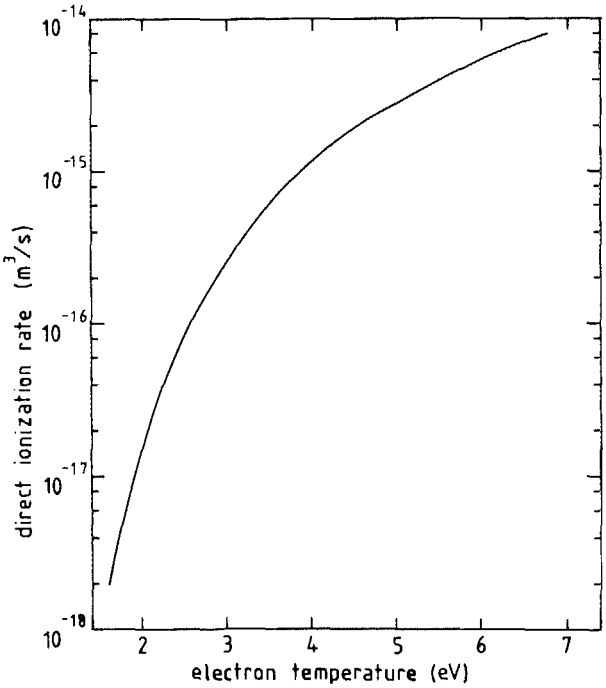

FIG. 1. The rate coefficient for the direct ionization of argon as a function of the electron temperature.

$$\langle \sigma v \rangle_{ia} = 1.66 \times 10^{-15} \sqrt{(\hat{T}_i / 1V)}\ (\text{m}^3/\text{s}). \tag{16}$$

We estimate the relative magnitude of neutral friction at $\hat{T}_i = 2$ V and $\hat{T}_e = 4$ V. Then $\langle \sigma v \rangle_{\text{total}} = \langle \sigma v \rangle_{ia} + \langle \sigma_{\text{ion}} v_e \rangle = 4.2 \times 10^{-15}$ m^3/s. Now for $\hat{n}_a \simeq 5 \times 10^{-2}$

$$\frac{M^a_{zi}}{(\partial / \partial z)p} \sim \frac{n_a \langle \sigma v \rangle_{\text{total}} w_{zi} Z}{v_{ti}^2} \lesssim 1. \tag{17}$$

E. Limitations in the validity of the model

The theoretical considerations are valid in the central core of the plasma where $\Omega_i \tau_{ii} < 1$. There the ion mean free path $l_{ii} \ll R$. At larger radii however the mean free path becomes of the order of the ion cyclotron radius $\rho_i = v_{ti} / \Omega_i$ which is not much smaller than R. The use of transport coefficients becomes invalid in that case.

Although we have only discussed classical transport theory, the influence of turbulent diffusion may be important under certain plasma conditions. We will recur to this in Sec. VI.

F. Numerical calculation

Scattering of the experimental data has a twofold cause. Not only random fluctuations occur but also long term drifts in the plasma parameters as a consequence of the finite lifetime of the cathode. Because we need to know the gradients in Eq. (6) with sufficient accuracy, we apply data reduction. Gaussian curves are chosen as the description of even radial profiles. This choice is well justified by the experiments. Some of the formulas used will be presented in the subsequent sections.

All formulas, with dependencies both on r and z, have been put into a computer program which calculates all terms of Eq. (6) for different values of r and z, using the experimentally determined values of w_{zi}, $w_{\theta i}$, T_e, T_i, n_e, and n_a.

III. EXPERIMENTAL ARRANGEMENT

The experiments have been carried out on a hollow-cathode argon arc with a tantalum cathode of 6 and 8 mm inner and outer diameter, respectively. The anode-cathode separation is 1.30 m. By longitudinal and sidewards displacement of the electrodes the arc is movable with respect to the diagnostics. For all the experiments a magnetic field of 0.2 T and an arc current of 50 A have been chosen.

The electron temperature T_e and density n_e are determined from Thomson scattering. The light source is a pulsed ruby laser (energy $\simeq$30 J, pulse duration $\simeq$1.5 ms). The scattered light is detected at a scattering angle of $\pi/2$ rad in five wavelength channels.[38,39] The sensitivity of the channels has been determined with respect to the sensitivity of a sixth channel at the central wavelength by the use of a tungsten ribbon lamp. Absolute calibration has been carried out by Rayleigh scattering from argon gas in the central channel. Near the cathode the fluctuations in the plasma background radiation do not permit accurate scattering measurements. In Fig. 2 the Abel inverted continuum intensity in one of the detection channels is plotted against n_e as measured with

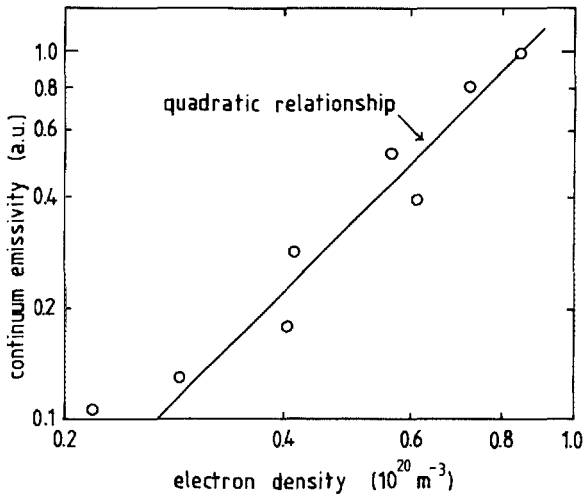

FIG. 2. The Abel inverted continuum emissivity as a function of the local electron density measured with Thomson scattering.

Thomson scattering. We see that the emissivity ϵ is proportional to n_e^2 with no significant influence of T_e. This proportionality agrees with the theoretical expectations.[38] Laterally scanned measurements of ϵ now provide the value of n_e in the case that Thomson scattering is not appropriate.

In the high-density range T_e is determined from the absolute intensity of the 488.0-nm ion spectral line. The population density n^* with respect to the ground state density n^0 behaves as

$$(n/g)^* = (n/g)^0 r^{(1)} \exp[-(E^* - E^0)/k_B T_e], \qquad (18)$$

where g denotes the statistical weight and $E^* - E^0$ the energy gap between the two levels. The collisional radiative coefficient $r^{(1)}$ of the Ar II $4p$ group is, according to model studies by van der Sijde,[40] in our parameter regime ($n_e > 3\times 10^{19}$ m^{-3}) nearly independent of n_e and depends only weakly on T_e. We have measured[40] $r^{(1)} = 4.5\times 10^{-4}$ at $n_e = 7.2\times 10^{19}$ m^{-3} and $\hat{T}_e = 3.3$ V.

With the known value of $r^{(1)}$, the T_e can be calculated with Eq. (18) from the population density n^* of the (Ar II $4p$ group) upper level of the 488.0-nm spectral line. In its turn the n^* follows from the measured absolute emissivity of this line.

The neutral particle density n_a is determined as follows. Once T_e is known, Eq. (18) can be used in the Ar I system to obtain the neutral ground-state density n_a^0 by measurements of the intensity of the 696.5-nm spectral line (upper level in the Ar I $4p$ group). For the Ar I $4p$ group the $r^{(1)}$ has been determined with the aid of the ion energy balance at the axis of the arc by Pots[39,41] for $\hat{T}_e \lesssim 4$ V:

$$n_a = \frac{0.25 n_e (1V)^2}{(\hat{T}_i - \hat{T}_a)[\hat{T}_i(\hat{T}_i + \hat{T}_a)]^{1/2}}. \qquad (19)$$

A value $r^{(1)} = 5.1\times 10^{-5}$ has been found.[35]

The temperatures of the ions T_i and of the neutrals T_a are measured from the Doppler broadening of spectral lines. We use the Ar I 696.5-nm and the Ar II 668.4-nm spectral lines. A monochromator is placed in tandem with a Fabry–Perot interferometer (FP). The FP is used in a central spot configuration and is wavelength scanned by variation of the argon gas density between the plates. The temperature of the FP is stabilized.[39]

Because of Zeeman splitting of the spectral lines, temperature measurements are performed with a Polaroid filter by which the π components are selected. We detect T_i and T_a using the radiation emerging at an angle of $\pi/2$ rad with the axis of the arc. Both spectral lines have upper and lower levels with slightly different Landé factors, so that some influence of Zeeman splitting remains. The absolute errors in T_i and T_a are about 0.1 eV.

The transmitted light intensity is measured with a photomultiplier and after amplification digitized in 256 samples. All data are stored and handled by a PDP 11 LSI computer. All measurements and calculations have been done with this computer, except Voigt deconvolutions of spectral lines for the determination of T_i and T_a. These are done with a Burroughs B7700 computer.

The drift velocities w_z and w_θ are measured along a line of sight (Fig. 3) at an angle α of 0.43 rad with the axis of the arc. In order to obtain an absolute wavelength shift $\Delta\lambda$ ($\Delta\lambda = 10^{-4}$ nm for a velocity of 45 m/s if $\lambda = 668.4$ nm) a reference beam has been used which emerges from the plasma oppositely to the primary beam and which after reflection and chopping returns to be detected together with the primary beam. A spectral red shift of the primary beam occurs together with a blue shift of equal magnitude in the secondary one. The multiplier signal is amplified and separated electronically into a dc and an ac component before digital storage (256 samples in a time of 60 s). The velocity measurements have been done with axial and lateral displacement of the plasma column in order to keep all optical paths unchanged. If in separated measurements the secondary beam is too noisy, this permits averaging over a number of spectral profiles.

A check of the setup with an unmagnetized gas discharge without gas flow has yielded a neutral particle drift velocity averaged over the line of sight as low as 20 ($\pm$ 10) m/s. Seeming wavelength shifts as a consequence of electronic averaging times during the wavelength scan have been excluded.

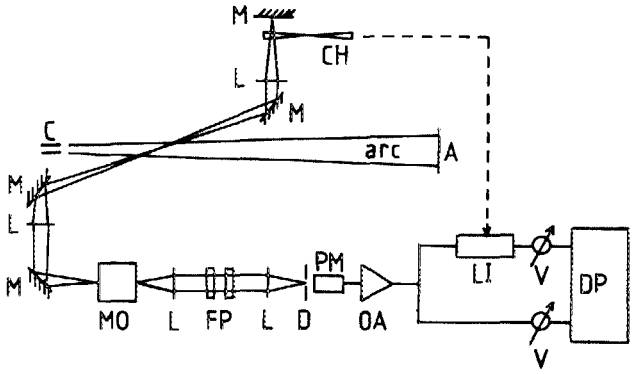

FIG. 3. Doppler shift diagnostic. C = cathode, A = anode, L = lens, M = mirror, CH = chopper, MO = monochromator, FP = Fabry–Perot interferometer plates, D = pinhole diaphragm, PM = photomultiplier tube, OA = operational amplifier, LI = lock-in amplifier, V = electrometer, DP = digital processing.

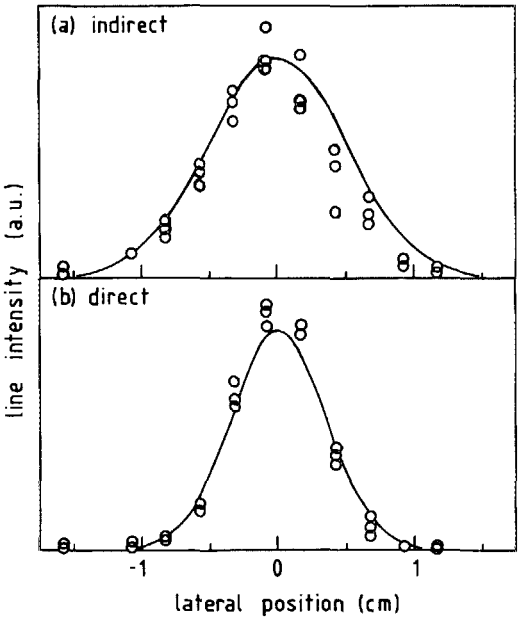

FIG. 4. Typical line intensities of the direct and the indirect beam as a function of the lateral position h. Longitudinal position $z = 10$ cm.

IV. MEASUREMENTS

For the calculation of local drift velocities from the line integrated ones, several wavelength scans have been performed at different lateral positions. The low intensity of the spectral lines confines us to positions near the axis of the arc. There in a good approximation we may write for the axial drift velocity w_{zi} and the rotation $w_{\theta i}$ of the ions:

$$w_{zi} = w_{z0i} \exp(-r^2/\lambda_z^2), \tag{20a}$$

$$w_{\theta i} = \omega r \exp(-r^2/\lambda_\theta^2), \tag{20b}$$

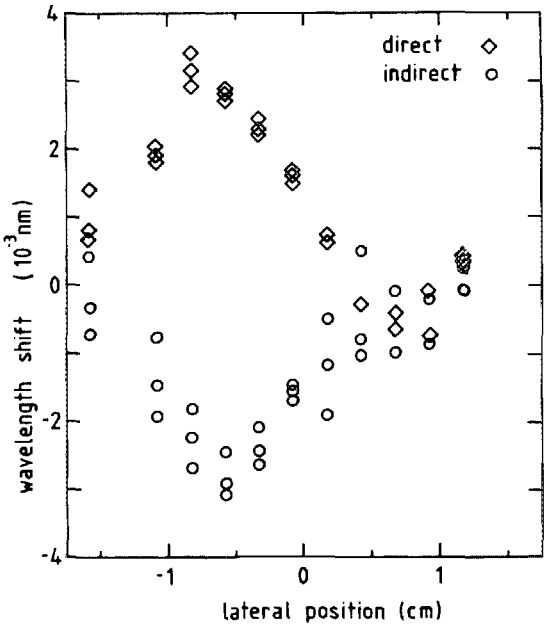

FIG. 5. Wavelength shifts of the Argon ion line at 668.4 nm as measured in the direct and in the indirect beam ($z = 10$ cm).

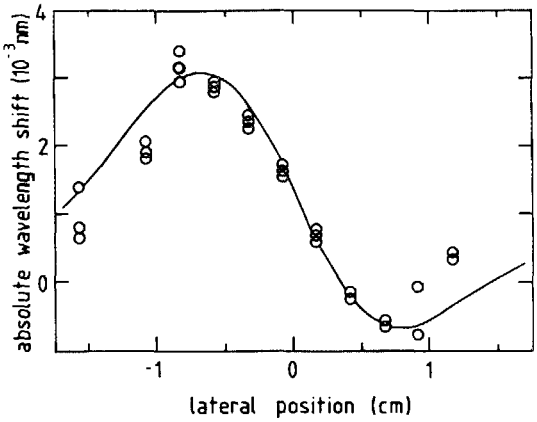

FIG. 6. Absolute wavelength shift of the Argon ion line at 668.4 nm with a least-squares-fitted curve according to Eq. (21) ($z = 10$ cm).

where w_{z0i}, λ_z, ω, and λ_θ are still dependent on the axial position z. The mean ion velocity $\langle w_i \rangle$, averaged over the line of sight, obeys

$$\langle w_i \rangle = \frac{-\omega h \sin(\alpha)\exp(-h^2/\lambda_\theta^2)}{(1+\lambda_I^2/\lambda_\theta^2)^{1/2}} + \frac{w_{z0i}\cos(\alpha)\exp(-h^2/\lambda_z^2)}{(1+\lambda_I^2/\lambda_z^2)^{1/2}}. \tag{21}$$

Here h is the lateral position of the detection beams (Fig. 4). We use the intensity I, which acts as a weight factor in the averaging, turns out to be a Gaussian function of r:

$$I = I_0 \exp(-r^2/\lambda_I^2). \tag{22}$$

In all our measurements $\lambda_I < \lambda_z$ and $\lambda_I < \lambda_\theta$. The corrections in the denominators of Eq. (21) amount to about 10%. In Eq. (21) the rotation appears as the odd part of $\langle w_i \rangle$ while the axial drift gives the even part in h. We note that $w_{\theta i}$ has a maximum:

$$w_{\theta i,\max} = \omega\lambda_\theta/(2e)^{1/2}, \tag{23}$$

where e is the base of the natural logarithms.

In Fig. 5 a typical wavelength shift as a function of h is given. A least-squares fit according to Eq. (21) is shown in Fig. 6. In this way the axial and rotational ion drifts have been determined at different positions z (Figs. 7 and 8). The arc parameters are mentioned in Table I. The rotation is composed of an E/B dominated drift and an oppositely directed diamagnetic drift. In the case of a strong B field ($\Omega_i \tau_{ii} \gg 1$) the diamagnetic drift $w_{di} \simeq v_{ti}\rho_i/R$ dominates, as has been reported on thermonuclear plasmas[42] (ρ_i is the ion

TABLE I. Parameters of the discharge.

Gas	Argon
Cathode	Tantalum; diameter: outer 8 mm, inner 6 mm
Neutral gas pressure	0.27 Pa
Gas flux	3.5×10^{20} s^{-1}
Magnetic field	0.2 T
Arc current	50 A
Arc length	1.3 m
Arc radius	$(1\text{–}2)\times10^{-2}$ m

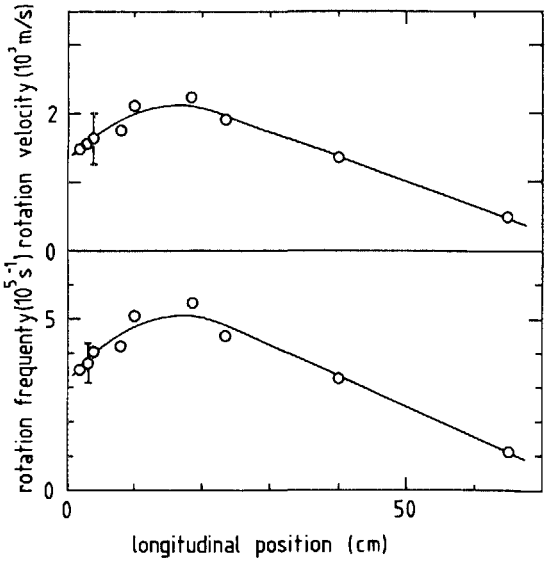

FIG. 7. The ion rotation at different longitudinal positions. Upper part: the maximal rotational velocity according to Eq. (23). Lower part: the angular rotation frequency (cathode at $z = 0$).

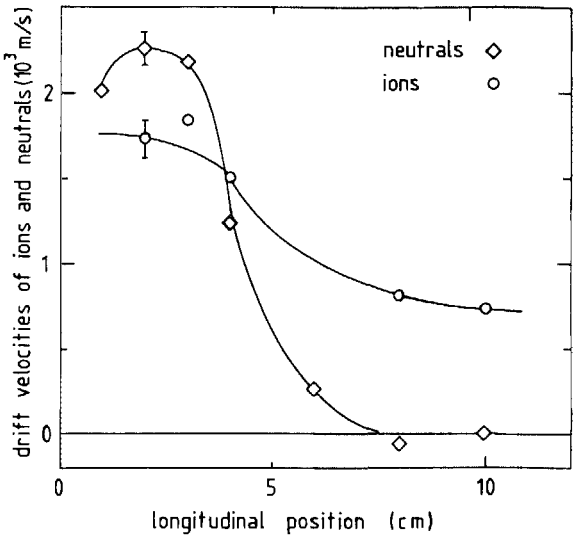

FIG. 9. Longitudinal drift velocities of ions and neutrals in the vicinity of the cathode.

cyclotron radius). We are dealing mainly with an E/B rotation w_{EBi}. Supposing that $E \simeq \hat{T}_e/R$, directed inward[29] and $w_{EBi} = E/B$, we expect $w_{EBi} \simeq -v_{ti}\rho_i/R$ also. The magnitude of $w_{\theta i,\max}$ is roughly between 30% and 50% of v_{ti}. Previously Timmermans *et al.* found values of about 30%.[28]

The axial ion velocity, the equivalent of the toroidal rotation in a tokamak,[23] reaches values of 500–1500 m/s at $z > 5$ cm but w_{z0i} is larger than 2000 m/s near the cathode, which indicates a sonic or near sonic expansion there.[37]

The neutral particle drift velocity decreases to zero within a few cm (Fig. 9). The neutral gas density near the cathode consists of two contributions.[43] A hot fraction expands with a considerable drift velocity from the cathode and a cold fraction without a measurable drift velocity emerges from the surrounding gas background. The change with increasing z in these fractions causes the w_{za} to decrease.

The characteristic widths are shown in Fig. 10. Near the axis the electron temperature as well as the density are approximately Gaussian functions of the radius:

$$T_e = T_{e0} \exp(-r^2/\lambda_{T_e}^2) \tag{24a}$$

$$n_e = n_{e0} \exp(-r^2/\lambda_{n_e}^2). \tag{24b}$$

A typical plot of Thomson scattering measurements is given in Fig. 11. n_{e0} and λ_{ne} are displayed in Fig. 12.

The ion temperature T_i as given in Fig. 13 turns out to be nearly independent of r.[28] We note that our values of T_i and T_e are in fair agreement with those of other authors.[44,28] The method of determining T_i by spectral line Doppler broadening has found its way also in thermonuclear plasma research.[45]

V. THE AXIAL MOMENTUM BALANCE

As stated before, a computer program has been written with which the numerical values of the different contributions to the axial momentum balance are calculated from the experimental data. The z dependencies of T_i, T_{e0}, n_{eo}, n_a, w_{z0i}, ω and the characteristic widths are fed into the program in the form of analytic representations. We only perform calculations at values of z larger than 5 cm. We have seen already that towards the periphery of the arc the theory becomes invalid.

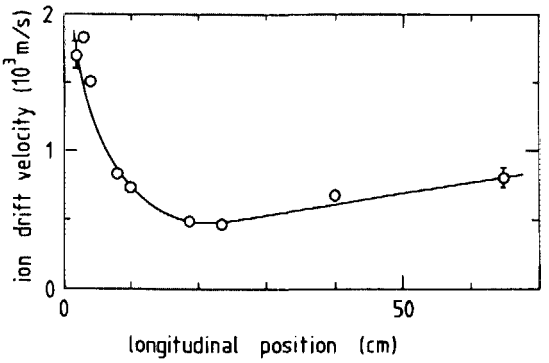

FIG. 8. Longitudinal ion drift velocity on the axis, directed towards the anode.

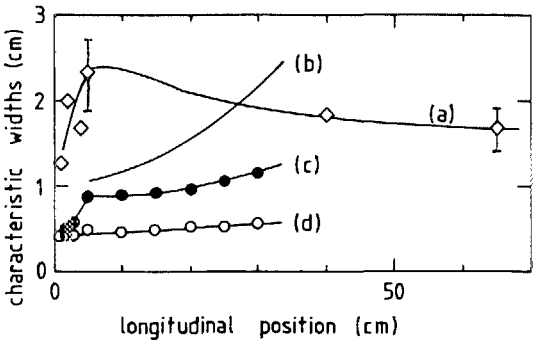

FIG. 10. Characteristic widths for the profiles of the longitudinal ion drift λ_z (a), the electron temperature λ_{T_e} (b), the Ar I $4p - 4s$ line (c) and the Ar II $4p$-$4s$ line (d).

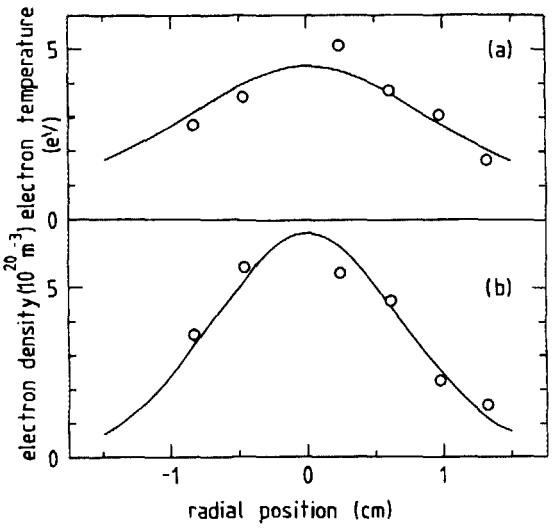

FIG. 11. Electron temperature (a) and the electron density (b) at $z = 30$ cm, measured by Thomson scattering.

The different calculated force densities at the axis of the arc are plotted in Fig. 14. A positive sign denotes an accelerating force density in the positive z direction. The inertia and the rotational contribution to the viscosity only play a role in the direct vicinity of the cathode. The neutral friction turns out to be of minor importance at the axis. Roughly the axial ion drift velocity is determined by the balance between the plasma pressure gradient and the kinematic viscosity. Because far from the axis $\Omega_i \tau_{ii} \gg 1$ and therefore the viscosity vanishes, there the neutral friction is expected to take over the decelerating force density from the viscosity. The viscosity only transfers momentum between inner and outer parts of the arc. It cannot add momentum to the plasma averaged over a cross section. We have experimental values of n_a only on the axis. We note that the viscosity in Fig. 14 does not compensate fully the pressure gradient. It is possible that turbulence may enhance the η coefficients.

Figure 15 shows the different terms in the axial momentum balance for different radii on a fixed z of 10 cm. All volume forces have been multiplied by r as a weight factor. We see that for values of r smaller than 0.5 cm the pressure gradient is balanced roughly by the ion viscosity. In the plasma edge the turbulence level has its maximum[39] and there the value of turbulent viscosity may exceed the kinetic one. We will estimate its magnitude.

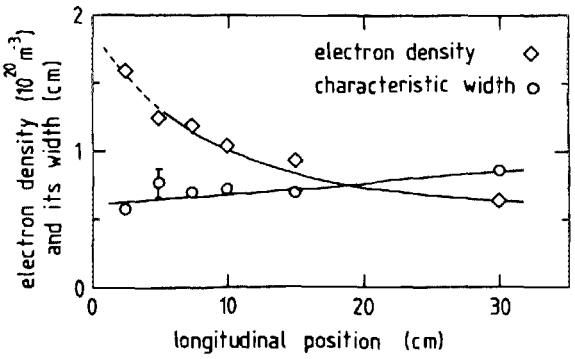

FIG. 12. The electron density on the axis and the characteristic width in radial direction of the electron density profile.

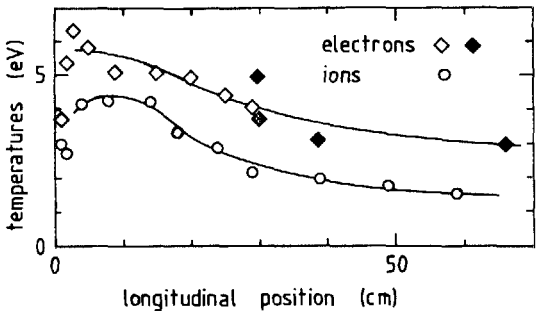

FIG. 13. The electron temperature and the ion temperature on the axis. The electron temperature is measured by optical spectroscopy (open diamond) and by Thomson scattering (closed diamond).

VI. THE INFLUENCE OF TURBULENCE

We are interested in the extent to which the ion viscosity η is enhanced by turbulence. In the foregoing we have seen that the kinematic ion viscosity η_2 fails to compensate fully the plasma pressure gradient. We investigate the turbulent viscosity coefficient η_t so that $\eta = \eta_2 + \eta_t$; $\eta_t \simeq n_i m_i D_t$, where D_t is the turbulent coefficient of self diffusion. For a full compensation of the pressure gradient by turbulent enhanced viscosity, the turbulent diffusion coefficient needs to be about 3 m^2/s. It has been argued[39,46] that the turbulence is caused mainly by a plasma flute instability with a logarithmic growth rate $\gamma = \alpha' w_{\theta i}/r$, with $\alpha' \simeq 10^{-1}$. In our case $\gamma \simeq 3 \times 10^4$ s^{-1}. Because the effective collision frequency ν_{ia} between the ions and the neutrals is sufficiently small, the instability is not collisionally damped and we are dealing with Bohm diffusion[20] so that $D_t \simeq \alpha' \hat{T}_e/B \simeq 2$ m^2/s, which value approaches the expected one.

Turbulently generated viscosity may play a role of at least the same importance as kinematic viscosity. The esti-

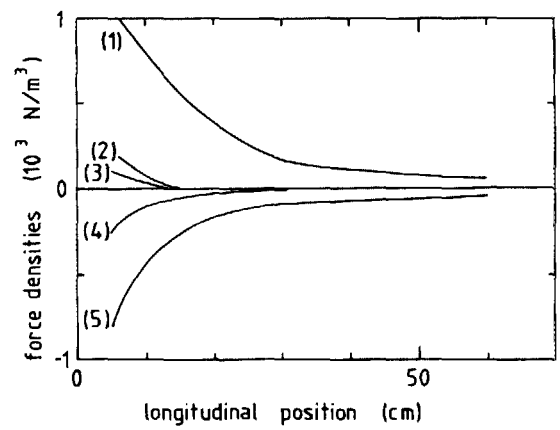

FIG. 14. The different force densities on the axis which contribute to the longitudinal momentum balance [Eq. (6)]. A positive sign denotes a force towards the anode; (1) pressure gradient, (2) viscosity including $w_{\theta i}$, (3) inertia with w_{zi} $(\partial/\partial z)\, w_{zi}$, (4) the friction of ions with neutrals and (5) viscosity including w_{zi}. The inertia term with w_{ri} $(\partial/\partial r)\, w_{zi}$ is too small to be visible in this figure.

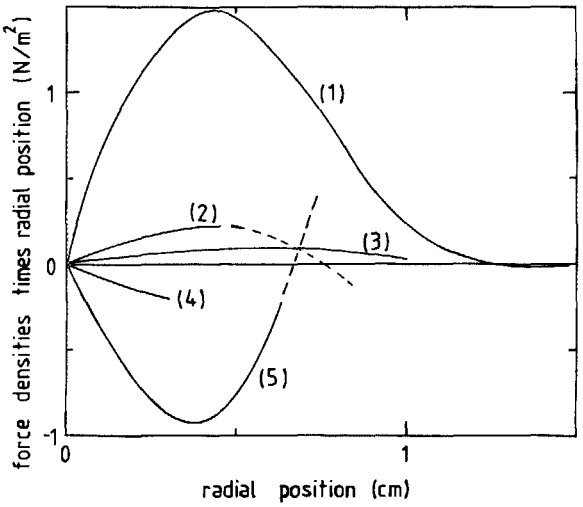

FIG. 15. The same force densities as in Fig. 14, multiplied with the radial position as a weight factor, over an arc cross section at $z = 10$ cm.

mates, although rough, are in fair agreement with the expected Bohm diffusion.

VII. CONCLUSIONS

The experimental data of w_{zi}, $w_{\theta i}$, n_e, n_a, T_e, and T_i, scanned over lateral and longitudinal positions, provide a good insight in the processes governing the axial ion drift. The Doppler shift spectroscopy with two detection beams has proven to be a reliable tool for measuring drift velocities. Because of the plasma pressure gradient the ions move towards the anode, against the direction of the electric field. The axial ion drift velocity w_{zi} decreases from a value of 2×10^3 m/s at the cathode to about a value of 5×10^2 m/s at $z = 20$ cm. There w_{zi} has a minimum and at the same longitudinal position the rotational velocity $w_{\theta i}$ reaches its maximum. The ion rotation amounts to a considerable fraction of the value of the ion thermal speed. The neutral particle density is composed of a fraction that leaves the cathode with the same longitudinal velocity as the ions, and the fraction that enters the arc from the surrounding gas background. In the first few centimeters near the cathode the former fraction causes the neutrals to drift, but further in the arc the neutrals are nearly without drift.

In the parameter range chosen for the arc the two dominant contributions in the axial momentum balance are the plasma pressure gradient and the ion viscosity, although at higher neutral background pressures also neutral friction plays a role. In the first few centimeters near the cathode other effects occur also: inertia and rotationally dependent viscosity. Although w_{zi} has a minumum at a position z of 20 cm, the plasma pressure decreases monotonously with z.

The classical transport theory gives quantitatively correct results, although its validity has two major limitations. In the outer region of the arc the ion Hall parameter $\Omega_i\tau_{ii}$ exceeds 1 while the gyration radius ρ_i approaches the arc radius. Furthermore turbulende generates Bohm diffusion, which causes an important turbulent contribution to the ion viscosity. The two major decelerating effects on the ions according to the classical theory can be expressed in two dimensionless numbers. The ratio of the ion viscosity to the plasma pressure gradient [Eq. (15)] is $(w_{zi}l_{ii}Z)/(v_{ti}R^2)$ and the ratio of the neutral friction to the plasma pressure gradient [Eq. (17)] is $n_a\langle\sigma v_i\rangle_{\text{total}}w_{zi}Z/v_{ii}^2$. From the values of these two numbers it can be decided whether viscosity or neutral friction dominates the deceleration and which magnitude of w_{zi} is to be expected.

Nevertheless, the effect of turbulence should be considered separately. Turbulent viscosity additionally transfers momentum between the plasma core and the outer region where it can be dissipated by neutral friction. Note also that the electron contribution to the gradient of the pressure essentially reflects the action of the ambipolar field.

[1] O. Klüber, Z. Naturforsch. Teil A **24**, 1473 (1969).
[2] O. Klüber, Z. Naturforsch. Teil A **27**, 652 (1972).
[3] P. A. E. M. Janssen and F. Boeschoten, Z. Naturforsch. Teil A **34**, 1022 (1979).
[4] P. A. E. M. Janssen and F. J. F. van Odenhoven, Physica (Utrecht) **98C**, 113 (1979).
[5] A. I. Karchevskii and E. P. Potanin, Sov. J. Plasma Phys. **8**, 101 (1982).
[6] A. I. Karchevskii, E. P. Potanin, A. A. Sarykin, and A. L. Ustinov, Sov. J. Plasma Phys. **8**, 172 (1982).
[7] M. Krishnan, M. Geva, and J. L. Hirshfield, Phys. Rev. Lett. **46**, 36 (1981).
[8] M. Geva, M. Krishnan, and J. L. Hirshfield, Nucl. Instrum. Methods **186**, 183 (1981).
[9] H. E. Wilhelm and S. H. Hong, J. Appl. Phys. **48**, 561 (1977).
[10] M. M. B. Wijnakker, E. H. A. Granneman, and J. Kistemaker, Z. Naturforsch. Teil. A, **34**, 672 (1979).
[11] M. S. van den Berg, Ph.D. thesis (Delft University of Technology, 1982) (unpublished).
[12] W. Ebert, Beitr. Plasma Phys. **19**, 281 (1979).
[13] J. P. C. Kroon, Ph.D. thesis (Eindhoven University of Technology, 1985) (unpublished).
[14] P. G. A. Theuws, H. C. W. Beijerinck, N. F. Verster, and D. C. Schram, J. Phys. E **15**, 573 (1982).
[15] P. G. A. Theuws, H. C. W. Beijerinck, D. C. Schram, and N. F. Verster, J. Appl. Phys. **48**, 2261 (1977).
[16] A. T. Forrester and J. M. Dawson, IEEE Trans. Plasma Sci. **PS-6**, 574 (1978).
[17] S. Tanaka, H. Morita, and J. Sakuraba, Jpn. J. Appl. Phys. **19**, 1703 (1980).
[18] A. I. Hershcovitch and V. J. Kovarik, Rev. Sci. Instrum. **54**, 328 (1983).
[19] A. I. Hershcovitch and K. Prelek, Rev. Sci. Instrum. **52**, 1459 (1981).
[20] J. M. M. J. Vogels and D. C. Schram (unpublished).
[21] J. M. M. J. Vogels, J. C. M. de Haas, B. Willems, T. Trommelen, and D. C. Schram, in *Proceedings and Contributed Papers of the International Conference on Plasma Physics*, edited by Hans Wilhelmsson and Jan Weiland (Chalmers University of Technology, Göteborg, Sweden, 1982), p. 11.
[22] V. V. Dyachenko, M. M. Larionov, A. D. Lebedev, L. S. Levin, and G. A. Serebreny, in *Contributed Papers of the 11th European Conference on Controlled Fusion and Plasma Physics* (European Physical Society, Aachen, F. R. G., 1983), p. E 35.
[23] R. C. Isler and L. E. Murray, Appl. Phys. Lett. **42**, 355 (1983).
[24] L. M. Lidsky, S. D. Rothleder, D. J. Rose, S. Yoshikawa, C. Michelson, and R. J. Mackin, J. Appl. Phys. **33**, 2490 (1962).
[25] J. L. Delcroix and A. R. Trindade, in *Advances in Electronics and Electron Physics*, Vol. 35 (Academic, New York, 1974).
[26] F. Boeschoten and L. J. Demeter, Plasma Phys. **10**, 391 (1968).
[27] F. Boeschoten, R. Komen, and A. F. C. Sens, Z. Naturforsch. Teil A, **34**, 1009 (1979).
[28] C. J. Timmermans, A. Lunk, and D. C. Schram, Beitr. Plasma Phys. **21**, 117 (1981).
[29] D. C. Schram, J. J. A. M. van der Mullen, B. F. M. Pots, and C. J. Timmermans, Z. Naturforsch. Teil A **38**, 289 (1983).
[30] S. I. Braginskii, in *Reviews of Plasma Physics*, Vol. I (Consultants Bureau, New York, 1965).
[31] K. Katsonis, Ph.D. thesis, Université Paris-Sud (1976).
[32] L. Spitzer, *Physics of Fully Ionized Gases* (Wiley-Interscience, New York, 1962).

[33]H. W. Drawin, Z. Phys. **164**, 513 (1961).
[34]J. J. A. M. van der Mullen, B. van der Sijde, B. F. M. Pots, and D. C. Schram, in *Proceedings of the International Conference on Phenomena in Ionized Gases* (Physical Society of the G. D. R., Berlin, 1977), pp. 323–324.
[35]B. van der Sijde, J. J. A. M. van der Mullen, and D. C. Schram, Beitr. Plasma Phys. **24**, 447 (1984).
[36]N. Kobayashi, J. Phys. Soc. Jpn. **38**, 519 (1975).
[37]P. G. A. Theuws, Ph.D. thesis (Eindhoven University of Technology, 1981) (unpublished).
[38]B. van der Sijde, S. Adema, J. C. M. de Haas, C. J. M. Denissen, and M. J. F. van der Sande, Beitr. Plasma Phys. **22**, 357 (1982).
[39]B. F. M. Pots, Ph.D. thesis (Eindhoven University of Technology, 1979) (unpublished).
[40]B. van der sijde, O. Abu-Zeid, and H. M. A. Wijshof, Phys. Lett. A. **101**, 491 (1984).
[41]B. F. M. Pots, P. van Hooff, D. C. Schram, and B. van der Sijde, Plasma Phys. **23**, 67 (1981).
[42]C. A. Kostek and T. C. Marshall, Plasma Phys. **25**, 421 (1983).
[43]J. M. M. J. Vogels, L. U. E. Konings, and D. C. Schram (unpublished).
[44]M. Bessenrodt-Weberpals, H. Kempkens, E. K. Souw, and J. Uhlenbusch, in *Contributed Papers of the XVIth International Conference on Phenomena in Ionized Gases*, edited by W. Boetticher, H. Wenk, and E. Schulz-Gulde (University of Düsseldorf, Düsseldorf, F. R. G., 1983), pp. 482, 483.